Original Research

Agro-Waste-Based Bio-Nanocomposite for the Mitigation of Pb (II) Ions from Water

Megha Gang[1], Awais Munir[2], Ghulam Murtaza[3], Rashid Iqbal[4]**, Asma Majeed[2], Muhammad Shoaib[2], Shweta Vyas[1]***, Iftikhar Ahmed[5], M. Irfan Akram[6], Zahra Ejaz[7], Allah Ditta[8,9]*, Waleed A. A. Alsakkaf[10], Jawaher Alkahtani[10]

[1] Department of Pure and Applied Chemistry, University of Kota, Rajasthan, India; meghagang30@gmail.com (M.G.); shwetavyas@uok.ac.in (S.V.)

[2] Institute of Agro-industry & Environment, The Islamia University of Bahawalpur, Pakistan; asma.majeed@iub.edu.pk (A.M.); awais.munir@iub.edu.pk (A.M.); muhammadshoaib.env@gmail.com (M.S.)

[3] Faculty of Environmental Science & Engineering, Kunming University of Science & Technology, Kunming 650500, China; murtazabotanist@gmail.com (G.M.)

[4] Department of Agronomy, Faculty of Agriculture and Environment, The Islamia University of Bahawalpur Pakistan; rashid.iqbal@iub.edu.pk (R.I.)

[5] Department of Soil Science, Faculty of Agriculture and Environment, The Islamia University of Bahawalpur Pakistan; iftikharahmedifii@gmail.com (I.A.)

[6] Department of Entomology, Faculty of Agriculture and Environment, The Islamia University of Bahawalpur Pakistan; drirfan@iub.edu.pk (M.I.A.)

[7] Institute of Biochemistry, Biotechnology & Bioinformatics, The Islamia University of Bahawalpur Pakistan; zahra.ejaz@iub.edu.pk (Z.E.)

[8] Department of Environmental Science, Shaheed Benazir Bhutto University, Sheringal 18000, Pakistan; allah.ditta@sbbu.edu.pk (A.D.)

[9] School of Biological Sciences, The University of Western Australia, 35 Stirling Highway, Perth, WA 6009, Australia

[10] Department of Botany and Microbiology, College of Science, King Saud University, Riyadh 11451, Saudi Arabia; walsakkaf.c@ksu.edu.sa (W.A.A.A.), jsalkahatani@gmail.com (J.A.)

Abstract

Plentiful quantities of agro-waste are generated after utilizing commercially valuable parts of the agro-biomass and often go to waste or are burned in the open air, resulting in environmental pollution. Herein, bio-nanocomposite is prepared using agro-waste-based activated carbon as a support and loading waste peel-mediated synthesized nanoparticles over it. The method used is cost-effective and simple due to its ease of synthesis and the availability of tons of agro-waste for sustainable agro-waste management. In the present work, orange peel extract is used to synthesize iron-oxide nanoparticles (IONPs) that are loaded over activated carbon derived from ice-apple fruit shell waste (IFSAC), based on the seventh principle of Green Chemistry. Batch studies were conducted using bio-nanocomposite to evaluate its adsorptive removal

* e-mail: allah.ditta@sbbu.edu.pk;
** e-mail: rashid.iqbal@iub.edu.pk;
*** e-mail: shwetavyas@uok.ac.in

efficiency for Pb (II) ions from water. The optimum conditions obtained for a Pb (II) ion concentration of 25 ppm were pH 5.5 at 40 °C for 120 minutes and stirring at 120 RPM. The maximum removal (99.44%) of Pb (II) at an adsorbent dosage of 0.2 g 10 mL^{-1} of bio-nanocomposite was achieved. Kinetics and thermodynamic parameters were also calculated to determine the viability of removal. The findings demonstrated that agro-wastes could be converted into useful assets for the sustainable development of the ecosystem, viz. ice-apple shell residue-derived nanocomposites (IONP@IFSAC) was verified to be a cost-effective adsorbent for the mitigation of lead from water.

Keywords: adsorptive removal, agro-wastes; bio-nanocomposite, iron oxide nanoparticles, Pb (II) ions removal

Introduction

In the current scenario, environmental pollution is increasing due to industrialization and hazardous chemical synthesis practices, so eco-friendly and greener procedures for technology development are becoming popular and highly appreciated worldwide. Numerous 'green chemistry' techniques have been adopted by researchers during the last decade, highlighting the basic and specific characteristics of green processes. Chemists and scientists globally now use the fundamentals of green chemistry as a common methodology when creating safe chemical reactions [1].

In the field of nanosciences, although conventional aerosol technology, UV irradiation, photochemical reduction, ultrasonic fields, laser ablation, and lithography methods have been proven effective in producing nanoparticles, they are still costly and require the use of harsh conditions and dangerous chemicals [2]. As a result, there is a great demand to create eco-friendly and sustainable methodologies for nanomaterial syntheses.

Many biological sources have been used to synthesize nanoparticles by various research groups due to their plentiful benefits over non-biological methods [3]. Utilization of biocompatible reagents in the preparation of nanoparticles reduced the toxicity of the final products and the environmental hazards of the by-products. Green solvents (ideally water) and "green" reagents like plant extracts have been employed to achieve this aim [4-8]. In the present work, we have utilized greener paths [9] to obtain iron oxide nanoparticles (IONP) and loaded this over-activated carbon (AC) to prepare ice apple fruit waste-activated carbon (IFSAC). Activated carbon is utilized as an adsorptive agent in separation and purification processes to decrease environmental pollutants in the air, water, and soil, which is of critical relevance in environmental pollution reduction [10]. The surface area of C, the pores internal structure, the surface properties, and functional groups existing on the adsorbent's surface all affect activated carbon's sorption capacity [11]. These criteria further depend on the technique of preparation used, as well as the precursor utilized. The creation of activated carbon from agricultural residues has been investigated by numerous researchers using bean peels, date palm fronds, apple pulp and apple peel, rice husk, pistachio hull, pistachio shell, apricot stone, hard cortex of apricot stones, spent tea leaves, banana peel, pineapple peel, dates kernels, residues of trimming peach trees, corn stalks, eucalyptus bark, etc. [12-14] Synthesized carbonized materials have been activated using physical activation or chemical activation methods [15]. Physical activation methods involve the preparation of activated carbon from any material rich in carbon contents to the extent of high temperatures of 700-1100°C under an inert gas atmosphere, followed by activation with agents like steam, oxygen, and carbon dioxide [16]. In the chemical activation approach, a comparatively lower temperature (400-700°C) is applied to carbonize the precursor materials by reacting them with chemical reagents, where carbonization and activation processes occur simultaneously [17]. There are several advantages to using a chemical activation approach rather than a physical activation method. The chemical approach is a low-cost process that can be completed in a single step at a lower temperature range with the generation of activated carbon in greater yields and a highly uniform pore structure [18, 19]. This approach of chemical activation has been used to synthesize activated carbons (ACs) by a large number of researchers, using a variety of chemical activating agents, viz. zinc chloride(ZnCl$_2$), hydrochloric acid (HCl), sodium hydroxide (NaOH), potassium hydroxide (KOH), hydrogen peroxide (H$_2$O$_2$), nitric acid (HNO$_3$), zinc chloride (ZnCl$_2$), phosphoric acid (H$_3$PO$_4$), etc. [20-24].

The present study aims to prepare orange peel extract-mediated IONPs for uploading over IFSAC to obtain bio-nanocomposite ice-apple shell residue-derived nanocomposites (IONP@IFSAC). Batch studies were directed to ascertain the ultimate adsorption capability of the synthesized bio-nanocomposite for eliminating lead from an aqueous medium. Lead has been extensively utilized for over 5000 years due to its corrosion resistance, high density, ductility, and malleability. Owing to its extensive use in paints, water pipes, acid storage batteries, protective coatings, construction supplies, glaze pigments, ceramics, crystals, glazers, and glass, as well as wine preservatives (halt fermentation), etc., flora and fauna found in aquatic environments [25, 26] and humans may consume lead through food daily and are exposed to Pb by-products [27], drinking-water [28], and inhalation [29]. Nevertheless, before the Industrial Revolution, lead exposure in the environment was very low; however, with industrialization and extensive mining, this exposure has increased [30]. Lead occurs in zero (0) and +2 oxidation

states as Pb (II) in the atmosphere, among which, the charged ionic form is more common and reactive. Looking into the hazardous effects of lead and its compounds, these are poisonous and bioaccumulating over time until a deadly dose is reached (a process known as cumulative poisoning). Lead poisoning in youngsters may cause cognitive problems, while it can cause progressive kidney illness in adults. Thus, many studies have been performed by researchers to mitigate Pb (II) from water [31-33].

Herein, nano-biosorbent is applied to eliminate Pb (II) from water, and studies are done to comprehend the effect of adsorbent dose/amount, temperature and pH, and the initial volume of the pollutant. The results showed the potential application of ice-apple shell residue-derived nanocomposites (IONP@IFSAC) for efficient abstraction of lead ions from water solutions.

Experimental

Materials

Sigma Aldrich made extra pure chemicals, viz. ferric chloride ($FeCl_3 \cdot 6H_2O$), sodium hydroxide (0.1M NaOH), hydrochloric acid (0.1M HCl), AAS Standard 1000 ppm solution of lead (Pb), deionized water, etc. Atomic Absorption Spectrophotometer (AAS-ice 3300, Thermoscientific), temperature control, and shaking were achieved by heating the mantle with a magnetic stirrer; a pH meter was applied to measure the solution's pH.

Preparation of Nano-Biosorbent

Pyrolysis of the ice apple fruit shell waste collected from local vendors was achieved with different alterations in the described method [34], in which air-dried biomass was dried in an oven at 383K (110 °C) for 24 hours, cooled, and stored in plastic bags. These were ground up, sieved to a 140-mesh size, and the fine powder was applied for activated carbon creation. The biomass samples were pre-carbonized for one hour at 300 °C in an electrical muffle furnace. After carbonization, the sample was directly impregnated with H_3PO_4 as a chemical activator. For this, carbonized samples (100 g) of IFS and 400 mL of H_3PO_4 (purity 85%) were mixed at a 10% concentration [35]. After stirring (700 rpm) at room temperature, the samples were put into an electric muffle furnace and heated for an hour at 900^0C in an inert nitrogen atmosphere. The generated activated carbon was collected and given time to cool to room temperature, before being stored in airtight bags to be kept in a desiccator. Iron-oxide nanoparticles (IONP) were made by continuously swirling 5 ml of freshly produced orange peel extract into a 50 mL solution (1 mM) of ferric chloride for fifteen minutes at 50 °C until a dark brown color solution was formed due to the decrease. Every thirty minutes, 50 ml of (1 mM) NaOH was mixed into the solution, resulting in a shift in color from dark brown to black, suggesting the development of the colloidal iron oxide ($Fe_xO_y.zOH$) nanoparticles. The obtained colloidal solution was centrifuged for 5 minutes at 4000 rpm in falcon tubes to attain solid iron oxide pellets, which were washed numerous times with cleansed water using a vertex mixer and centrifuged for 10 minutes at 4500 rpm, after which the supernatant water was eliminated through decantation. After washing, the material was dried in an oven at 80 °C for 2h before being calcined in a furnace at 450 °C for 5 hours. Loading of magnetite nanoparticles (IONP) on IFSAC was performed by adopting the conventional immersion method with slight changes. To ensure uniform mixing, the finely ground 1.0 g IONPs were added with 10 ml of double-cleansed water, and 1.0 g IFSAC was added. The mixture was vigorously agitated for two hours. Filtration
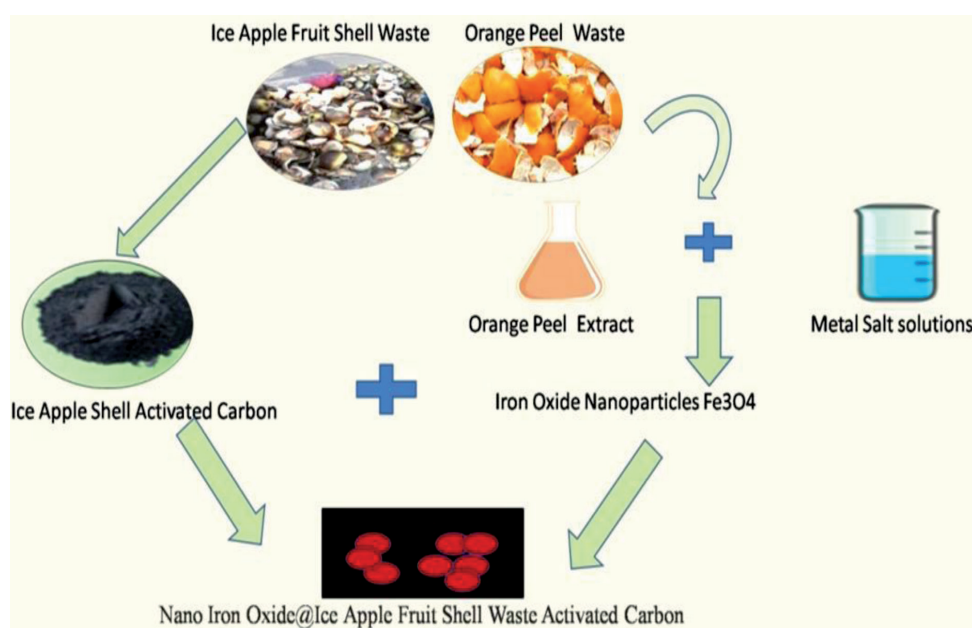

Fig. 1. Schematic presentation of synthesis of IONP@IFSAC

and decantation were used to eliminate the liquid from the resulting black slurry, and multiple washes with double-distilled water were performed on the solid. The resulting precipitate was dried in a muffle furnace for two hours at 500 °C and twelve hours at 90 °C to create the inexpensive and environmentally beneficial bio-nanocomposite ice-apple shell residue-derived nanocomposites (IONP@IFSAC), which is shown in Figure 1.

Characterizations

Determination of the Moisture Content

As moisture adsorbed on the surface impacts the sorption efficacy of the adsorbent, it is essential to ensure the amount of moisture before running any batch experiment. This was determined by weighing 5 grams of bio-nanocomposite into a previously weighed pot, placing it in an oven, and heating it for 5 hours at 105 °C. The prepared sample was taken out and quickly placed in a desiccator to stop it from absorbing moisture, and it was then weighed again. This process was carried out multiple times until a steady weight was achieved. The adsorbent's moisture content is determined by the mass differential equation 1.

$$\% \text{ Moisture content} = \frac{w2-w3}{w2-w1} \times 100 \qquad (1)$$

W1 = Weight of vessel, W2 = Initial weight of vessel with sample, W3 = Final weight of vessel sample

Determination of Surface Properties

Different techniques, like SEM, TEM, FTIR, and XRD, are applied to test the structural properties of the created bio-nanocomposite IONP@IFSAC and found to be comparable with studies performed by earlier research groups [36-40]. SEM images demonstrated that the IONP nanoparticles have been stuck to each other as well as to the IFSAC surface to give a rough, porous, and coarse structure with the grooves of IFSAC (Figure 2). The TEM image showed a spherical shape of iron oxide particles, with some in cubic shape (Figure 2). The size of IONP@IFSAC was in the range of 20-100 nm with spherical structures, which is inconsistent with the results of the XRD investigations. XRD studies confirmed the
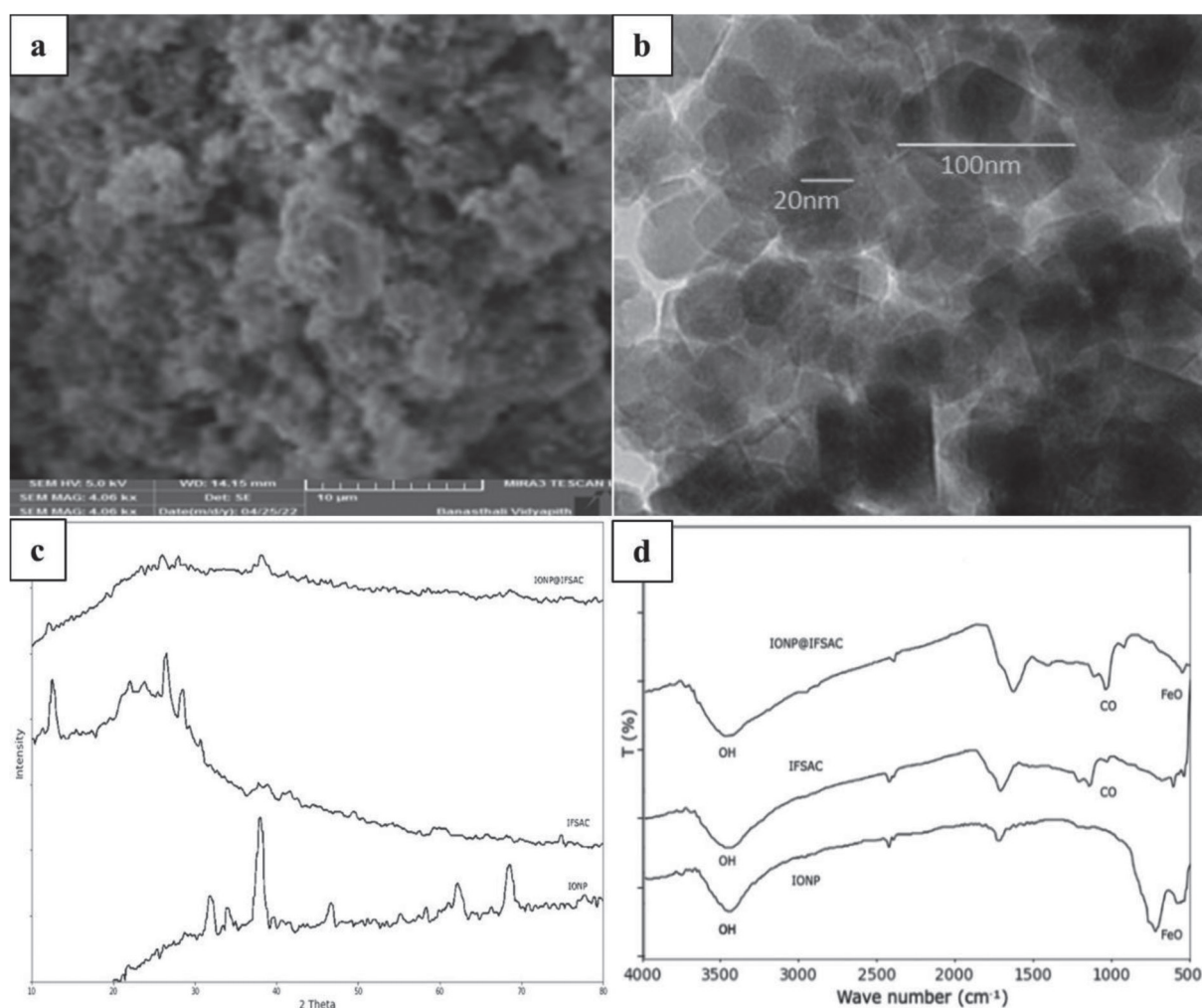

Fig. 2. Characterization of IONP@IFSAC by a) SEM b) TEM c) XRD d) FTIR

formation of IONP in the form of Fe_3O_4 showing 2θ peak values between 31.20°, 36.19°, 44.26°, 53.25°, 58.32°, 64.28°, and 76.54°, corresponding to diffraction planes (HKL) of 220, 311, 400, 422, 511, 440, and 533, respectively, indicating the crystalline structure of IONP (Figure 2). After loading IONP over IFSAC, these peaks lost intensity, which indicated the formation of crystalline or amorphous bio-nanocomposite material. FTIR studies also supported the appearance of –OH, -COOH, -C=O, etc. functional groups with a decrease in Fe-O stretching intensity, hence confirming the loading of IONP on the IFSAC to form a biocomposite material.

Results and Discussion

Adsorptive Removal of Pb (II) by Bio-Nanocomposite IONP@IFSAC

Studies in batches were conducted to examine the sorption ability of IONP@IFSAC at various dosages, reaction times, pHs, temperatures, and concentrations of metal ions [36] with continuous stirring to ensure homogenous mixing. After the predetermined amount of time, the flask containing the sample was taken out, and the leftover metal ion concentrations were measured using an atomic absorption spectrophotometer. Langmuir and Freundlich's models were tested to analyze the sorption data, and their constants were assessed [37]Triticum aestivum, in an aqueous system were investigated. Among the models tested, namely the Langmuir, Freundlich, Temkin, and Dubinin-Radushkevich isotherms, the biosorption equilibrium for both Cd2+ and Cu2+ was best described by the Langmuir model. The Langmuir biosorption capacity for Cd2+ was about 27% higher than that for Cu2+. It was also found that biosorption of Cd2+ and Cu2+ by wheat straw followed second-order kinetics. The equilibrium amount of metal ions adsorbed onto the wheat straw increased with increasing of pH from 4.0 to 7.0, and the effect was more pronounced for Cd2+ than for Cu2+. The equilibrium adsorbed amount also increased with the initial concentration of the metal ions, as expected. On the other hand, an increase of temperature from 25 to 30 °C only enhanced the biosorption of Cd2+ and Cu2+ slightly. The apparent temperature independence and the strong pH dependence of the amount of metal ions adsorbed along with moderate mean free energies of biosorption (between 8.0 and 12.9 kJ mol-1. To examine the influence of different parameters/factors including pH, the initial amount of adsorbate (C0) and reaction time (t) on the sorptive elimination of heavy metal ions, batch studies were done [32]Triticum aestivum, in an aqueous system were investigated. Among the models tested, namely the Langmuir, Freundlich, Temkin, and Dubinin-Radushkevich isotherms, the biosorption equilibrium for both Cd2+ and Cu2+ was best described by the Langmuir model. The Langmuir biosorption capacity for Cd2+ was about 27% higher than that for Cu2+. It was also found that biosorption of Cd2+ and Cu2+ by wheat

straw followed second-order kinetics. The equilibrium amount of metal ions adsorbed onto the wheat straw increased with increasing of pH from 4.0 to 7.0, and the effect was more pronounced for Cd2+ than for Cu2+. The equilibrium adsorbed amount also increased with the initial concentration of the metal ions, as expected. On the other hand, an increase of temperature from 25 to 30 °C only enhanced the biosorption of Cd2+ and Cu2+ slightly. The apparent temperature independence and the strong pH dependence of the amount of metal ions adsorbed along with moderate mean free energies of biosorption (between 8.0 and 12.9 kJ mol-1. By applying a well-established relation to the discrepancies between the amount of the initial and final solute in the solution before and after sorption, the solute's amounts sorbed per unit mass of adsorbent (Qe) were determined by equation 2:

$$Qe = (C_o - C_e)\, V/W \qquad (2)$$

Where V represents the volume of the sample, measured in liters, the variable C represents the initial concentration of the solute, measured in milligrams per liter (mg L-1), the variable "Ce" represents the concentration at equilibrium, measured in milligrams per liter (mg L-1), and W is the dry weight of the adsorbent in grams. The thermodynamics and kinetics of the adsorption of lead ions on adsorbents were assessed using a process similar to our earlier run of experiments, which was described by many other researchers [38-40]

In 50 ml of synthetic wastewater with (Pb II) ion concentrations, batch tests were performed to investigate the adsorption capability of IONP@IFSAC (1g) at different temperatures, contact times, and pH levels as per previous study patterns, with continuous stirring to ensure homogenous mixing as indicated in Table 1. The data on sorption were analyzed by applying the Freundlich and Langmuir models, and their constants were evaluated [41]

The flask comprising the remaining lead ions was withdrawn at the desired time interval and examined through an Atomic Absorption Spectrophotometer (AAS, Ice 3300 Thermofischer Scientific) for equilibrium Pb (II) ion concentrations. The batch experiments were repeated with different parameter sets. To test the reproducibility and to account for sorption onto the inside glass bottle surface, blank samples were used without adsorbent under comparable amounts, temperatures, and pHs. The experiments were conducted in triplicate.

Effect of Temperature

The impact of temperature on the abstraction of lead through NIO@IFSAC nano-composite was examined over a temperature between 20 and 40 °C using a fixed dose (1g 50 mL-1), and pH 5.5 at 10 ppm lead ion conc., mixing at 120 rpm for 120 min. The sorption efficacy of the adsorbent was elevated initially by increasing temperature and found its maximum at 30 °C, indicating that the reaction follows the endothermic pathway;

Table 1. Batch experimental parameters for batch reaction conditions

Parameters	Units	Range
Pb(II) concentration	ppm	05-30
pH	-	02-08
Contact time	Minutes	20–180
Temperature	°C	20-40
Adsorbent dose	g L^{-1}	04-20

however, with more increments in temperature, desorption started at much higher levels.

Effect of Time and Initial Concentration of Pb (II) Ions on Adsorption

By changing the reaction time from 20 to 180 minutes, the impact of volume and reaction time on the uptake of Pb (II) ions was inspected (Figure 3). The time was increased quickly between 20 and 120 minutes, becoming constant when impending saturation as equilibrium was achieved, the maximum removal percentage for lead was found to be 94.6% at 120 minutes for a 10 ppm volume of lead ions.

Effect of Adsorbent Dosage

The adsorptive abstraction of lead from an aqueous medium concerning the adsorbent amount is shown in Figure 4. The quantity of nano-adsorbent differs from 4 g/L to 20 g/L keeping all other parameters constant throughout the initial amount (25 ppm), pH 6, and reaction time of 120 minutes. At 120 RPM, it is evident that there is a constant surge in the percentage abstraction of Pb (II) metal, with enhancing the adsorbent amount as more binding sites are available, so a continuous increase in removal efficiency is observed. The maximum removal efficiency of 99.44% is obtained at the time of 120 min., which may be expected due to the establishment of equilibrium; hence, further increasing time does not affect the removal efficiency.

Effect of pH on Adsorption of Pb (II) Ions

The pH of the solution governs the surface charges of the adsorbent and the chemistry of the binding of metal ions; thus, it is a critical factor that significantly influences the sorption process (Figure 5). The influence of the pH on the elimination of lead ions (10 mg L^{-1}) via adsorbent (0.250 g 50 mL^{-1}) was carried out. As the solution's pH rises from 1 to 6, the sorption ratio of lead ions increases from 58 to 93%, representing optimum sorption at 5.5 pH. At a pH higher than six, the formation of hydroxides of lead occurred, which caused precipitation.

Studies on Adsorption Isotherms

A sorption isotherm is a plot that shows the connection between the quantity of the adsorbate at equilibrium and the amount of adsorbate that is adsorbed at a fixed temperature. The sorption process has been studied using many sorption isotherms, with the Freundlich and Langmuir models being the most often used owing to their ease and ability to accurately represent experimental data across a varied range of volumes [42-45]Triticum aestivum, in an aqueous system were investigated. Among the models tested, namely the Langmuir, Freundlich, Temkin, and Dubinin-Radushkevich isotherms, the biosorption equilibrium for both Cd2+ and Cu2+ was best described by the Langmuir model. The Langmuir biosorption capacity for Cd2+ was about 27% higher than that for Cu2+. It was also found that biosorption of Cd2+ and Cu2+ by wheat straw followed second-order kinetics. The equilibrium amount of metal ions adsorbed onto the wheat straw increased with increasing of pH from 4.0 to 7.0, and the effect was more pronounced for Cd2+ than for Cu2+. The equilibrium adsorbed amount also increased with the initial concentration of the metal ions, as expected. On the other hand, an increase of temperature from 25 to 30 °C only enhanced the biosorption of Cd2+ and Cu2+ slightly. The apparent temperature independence and the strong pH dependence of the amount of metal ions adsorbed along with moderate mean free energies of biosorption (between 8.0 and 12.9 kJ mol-1. In this case, the Freundlich model is related to a heterogeneous surface of sorption with a non-uniform circulation of the heat of sorption, whereas the Langmuir isotherm refers to homogeneous monolayer sorption. These models are used to illustrate equilibrium sorption and evaluate sorption capacities [46]

Kinetic Rate Constant

The first-order rate formulation provided by Lagergren was used to get the kinetic rate constant (Kad) for sorption by equation 3.

$$\ln(q_e - q_t) = \ln(q_e) - kt \qquad (3)$$

In this context, qe (mg/g) represents the sorption volume of the nano-adsorbent for heavy metal ions at equilibrium, while qt (mg/g) represents the sorption volume at any given time t (in minutes). The rate constant of the pseudo-first-order kinetic model is denoted k (1/min). A linear chart of the natural logarithm of the difference between qe and qt, versus time (t), was utilized to get the rate constant (k). The determination coefficient (R) was also determined.

Langmuir Isotherm Studies

The Langmuir model applies to sorption on fully homogeneous surfaces, where there is minimal interaction between the molecules that are being adsorbed (Figure 6). Equation 4 represents the linearized form of the Langmuir isotherm model, as follows:

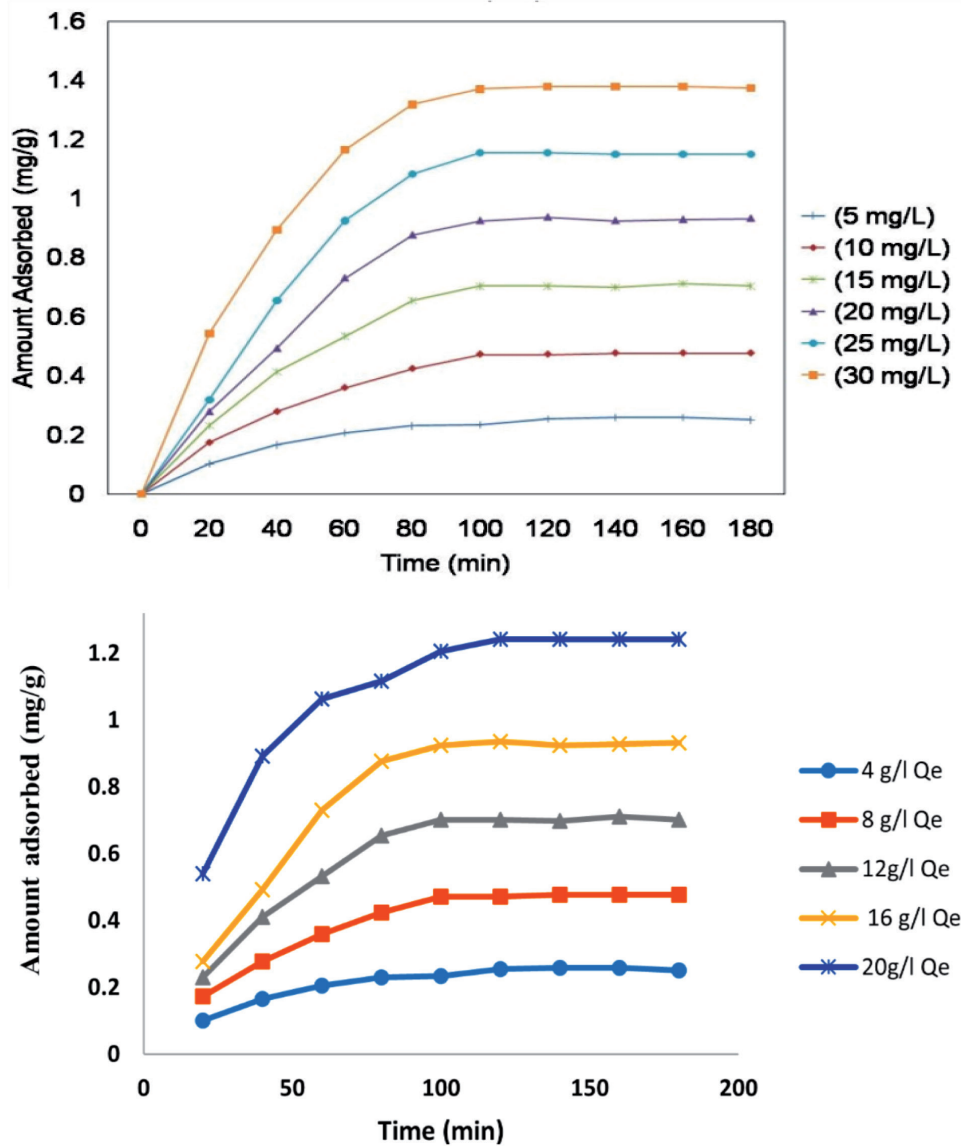$$\frac{Ce}{qe} = \frac{1}{q\,max * KL} + \frac{Ce}{qmax} \qquad (4)$$

Fig. 3. Effect of time and initial concentration of Pb(II) ions on adsorption

The variable Ce (mg/L) represents the equilibrium concentration of the adsorbate in the solution. The variable qe (mg/g) represents the adsorption capacity of metal ions on the adsorbents at equilibrium. The variable qmax (mg/g) represents the highest monolayer sorption ability of metal ions on the adsorbents. The Langmuir isotherm constant KL (expressed in L/mg) is a parameter that quantifies the relationship between the free energy of sorption and the sorption process. The values of qmax and KL can be determined by analyzing the intercept and slope of the linearized Langmuir equation. The fundamental attributes of the Langmuir isotherm can be articulated with a non-dimensional constant separation factor, RL, as defined in equation 5.

$$R_L = \frac{1}{1 + K_L C0} \qquad (5)$$

Where C_o (mg/L) is the initial conc. of lead ions in aqueous. The sorption is measured favorably when $0 < R_L < 1$.

The K_L values (min^{-1}) were computed from slopes of linear plots of log ($q_e - q_t$) vs. time (t) at 293K, 303K, and 313K for Pb II and found (0.120), (0.542), and (0.246) which indicated the highest adsorption at 303K with q max 1.78 mg/g. The high correlation coefficients ($R^2 = 0.999$) show that sorption follows first-order kinetics.

Freundlich Isotherm Studies

The Freundlich isotherm model is an extensively recognized equation applied to explain sorption on surfaces that have different properties. It predicts that the energy required for sorption reduces exponentially as the sorption center of an adsorbent becomes more saturated (Figure 7). The empirical model employed in this study describes the process of sorption in aquatic media. It is utilized to elucidate the detected phenomenon of Pb (II) ion adsorption on bio-nanocomposites. The
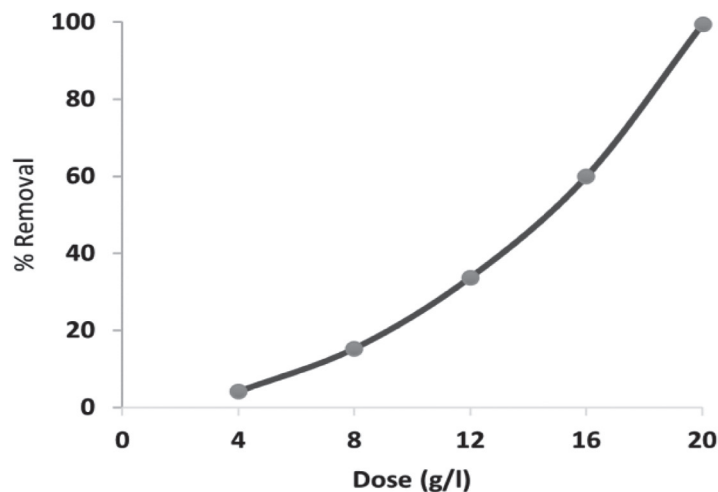
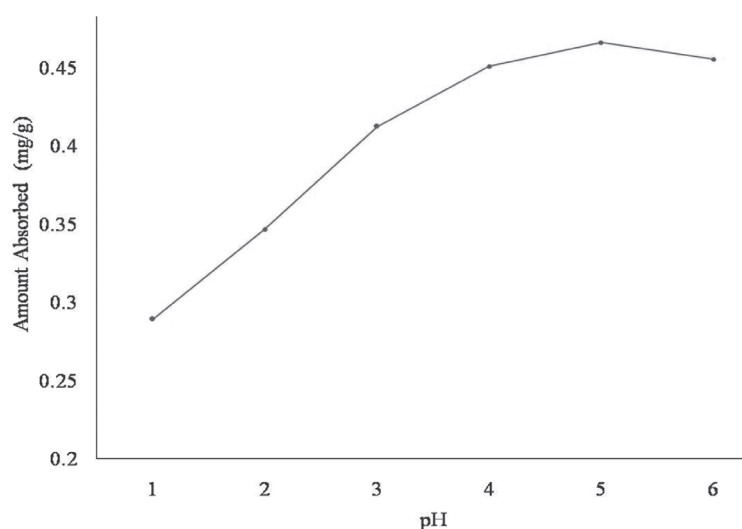Fig. 4. Effect of adsorbate dose on Pb(II) ions adsorption

Fig. 5. Effect of pH on adsorption of Pb(II) ion

linear form of the Freundlich model can be expressed in Equation 6:

$$\ln q_e = \ln K_F + 1/n \ln C_e \qquad (6)$$

Freundlich variables, KF (mg/g) and (L/mg), 1/n represent the sorption ability and sorption strength, respectively. The values of the Freundlich model's parameters, KF and 1/n, can be determined by analyzing the intercept and slope of the linearized form of the model's equation (Table 2).

Thermodynamic Studies

Thermodynamic analyses are necessary to examine the possibility, natural occurrence, heat of sorption, and specific type of sorption, as well as the physiochemical and other mechanisms involved. The Van't Hoff calculation was employed to estimate the thermodynamic factors of entropy ($\Delta S°$) and standard enthalpy ($\Delta H°$) for the sorption mechanism using equations 7 and 8.

$$\ln K_L = \Delta S°/R - \Delta H°/RT \qquad (7)$$

$$\Delta G = -RT \ln K_L \qquad (8)$$

The Langmuir constant, denoted as KL (in units of L mol-1), is a parameter in the Langmuir equation. The gas constant, denoted as R (with a value of 8.314 J mol-1 K-1), is a fundamental constant in thermodynamics. The symbol T represents the absolute temperature in Kelvin (K). The KL values obtained from the Langmuir model at various temperatures were utilized to determine thermodynamic factors, including the change in Gibbs free energy ($\Delta G°$). The results of enthalpy change ($\Delta H°$) and entropy change ($\Delta S°$) can be determined by calculating the intercept and slope of the linear graph obtained by plotting the natural logarithm of the equilibrium constant (ln KL) against the equal of
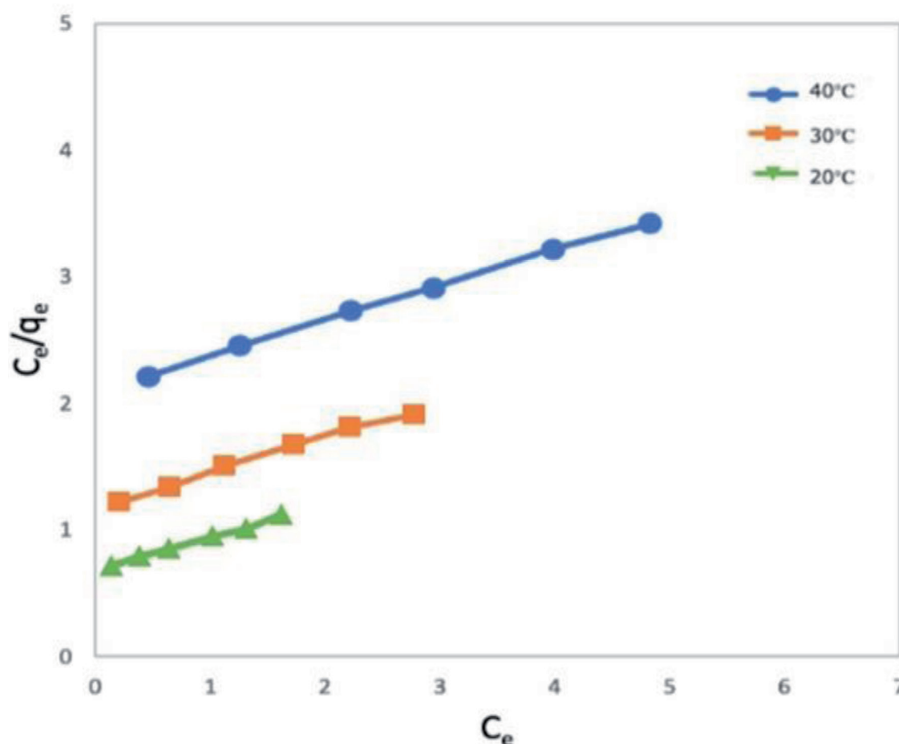
Fig. 6. Langmuir plots for Pb(II) ion removal at different temperatures

Table 2. Langmuir and Freundlich isotherms data for adsorption of Pb (II) ions on IONP@IFSAC at different temperatures

Adsorbate	Temperature	Langmuir	Constants	Freundlich	Constants
Metal ions	(°C)	$Q°$ (mg g^{-1})	b (L mg^{-1})	K_F (mg g^{-1})	1/n
Pb(II)	20	3.20	0.131	0.368	0.794
	30	3.44	0.249	0.658	0.795
	40	3.53	0.413	1.010	0.804

temperature (1/T). The negative values of $\Delta G°$ advocate the feasibility of sorption of the metal ions onto IONP@AC in a spontaneous and favorable process (Table 3). It is well known that physical adsorption can occur if the result of $\Delta G°$ is ≤ 8.0 KJ mol^{-1} and for chemical sorption, its value is between 20 and 40 KJ mol^{-1}. The ΔGo, $\Delta H°$, and $\Delta S°$ are computed to determine the standard free energy change, enthalpy change, and entropy change, respectively. The $\Delta G°$ (KJ/Mol) values for Pb (II) range from 0.875 to 4.642, suggesting that physisorption is occurring. The $\Delta G°$ values become increasingly negative as the temperature increases, indicating that the removal process is more favorable at higher temperatures. Positive values of $\Delta H°$ 39.9–47.78 between 20 and 40 °C indicate that the sorption procedure is endothermic. The rise in ΔSo values as temperature increases indicates a greater level of disorder at the interface between the solid and the liquid during the process of sorption.

The batch experiments were successfully actioned for the determination of optimization and understanding of the kinetic parameters. The relationship between Ce/qe and Ce follows a linear pattern, indicating that the Langmuir equation is valid. This suggests that there is monolayer coverage on the unit mass of adsorbent (mg g-1) and that the adsorption process is endothermic. The high correlation coefficients (R^2) indicated a strong correlation (0.98–0.99) and conformed to pseudo-first-order kinetics. The applicability of the Freundlich model was confirmed by the data obtained through a linear plot of log qe versus log Ce. The correlation coefficients ($R^2 = 0.89$–0.91) suggest that the data aligns more closely with the Langmuir model than the Freundlich model. Therefore, the adsorption process of Pb (II) onto IONP@IFSAC is considered to follow both paths, but more suitably, the Langmuir isotherm is fitted. The sorption capacity for Pb(II) ions exhibited an increase from 82% to 98% as the temperature was raised from 20 to 40 °C. This suggests that the sorption process is endothermic, in line with diffusion-controlled adsorption. At elevated temperatures, the movement of the adsorbate is made easier, in addition to an increase in the number of adsorption sites formed as a result of the disruption of a few internal bonds around the periphery of the active surface.
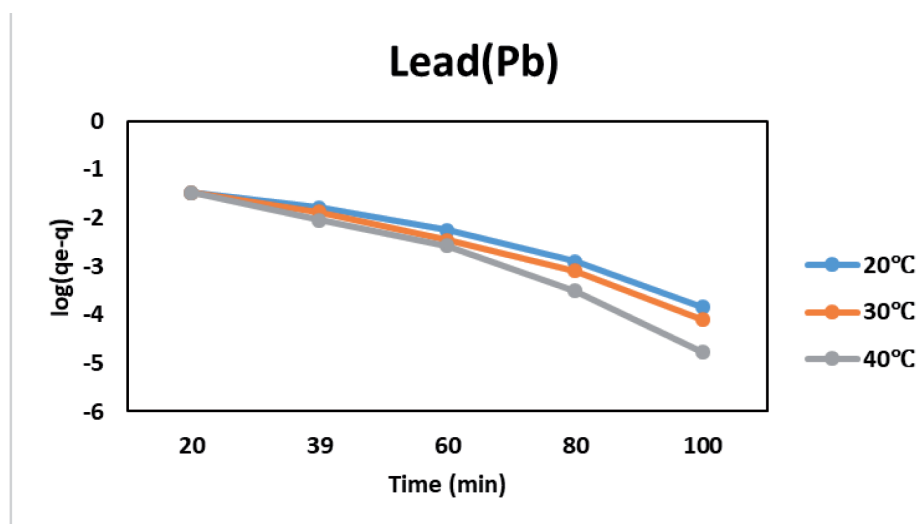
Fig. 7. Freundlich Adsorption for Pb(II) metal ion removal at different temperatures

Table 3. Thermodynamic parameter for adsorption of Lead ions Pb (II) on IONP@IFSAC at different temperatures

Metal	Temp, K	-ΔG° kJ/mol	ΔH° kJ/mol	ΔS° J/Kmol	R^2
	293	0.875	39.9	216	0.918
Pb(II)	303	2.971	42.8	228	0.999
	313	4.642	47.7	242	0.990

Conclusions

Agrowaste-based bio-nanocomposites were successfully prepared by a greener route, characterized by SEM, TEM, FTIR, and XRD analysis, and utilized for the effective elimination of lead ions in aqueous media. The current study confirmed that IONP has been loaded on IFSAC, and adsorption of lead ions onto bio-nanocomposite can be achieved at a maximum of 25 ppm of lead ions with a maximum removal efficiency of 99.44% at 5.5 pH and an adsorbent amount of 0.2 g 100 mL^{-1}. The findings of the current study demonstrated that sorption was spontaneous, multi-layered, as evidenced by the Langmuir and Freundlich models, and endothermic, as elimination efficacy can be enhanced by raising the temperature. Therefore, agro-waste-based bio-nanocomposites could be utilized as an efficient adsorbent for the elimination of similar toxic heavy metal contaminants from aqueous media.

Acknowledgments

Conflict of Interest

The authors declare no conflict of interest.

References and Notes

1. ABBAS G., BATOOL F., AHMED A., WAGI S., GONDAL H.Y., MAQSOOD F., ABDELRAHMAN E.A., NAEEM H.K., KANWAL S., MUSTAQEEM M., DITTA A. Green synthesized silver nanoparticles: Characterization, phytostimulatory impacts, and degradation potential for organic pollutants. Biocatalysis and Agricultural Biotechnology **55**, 102993, **2024**.
2. JIANG S.Z., LI L., HUANG H., HE W., MING W. Progress in Laser Ablation and Biological Synthesis Processes: "Top-Down" and "Bottom-Up" Approaches for the Green Synthesis of Au/Ag Nanoparticles. International Journal of Molecular Sciences, **23,** 14658, **2022**.
3. KANWAL S., NAEEM H.K., BATOOL F., MIRZA A., ABDELRAHMAN E.A., SHARIF G., MAQSOOD F., MUSTAQEEM M., DITTA A. Adsorption potential of orange rind-based nanosorbents for the removal of cadmium (II) and chromium (VI) from contaminated water. Environmental Science and Pollution Research, **30**, 110658, **2023**.
4. MONDAL P., ANWESHAN A., PURKAIT M.K. Green synthesis and environmental application of iron-based nanomaterials and nanocomposite: A review. Chemosphere, **259**, 127509, **2020**.
5. MARSLIN G., SIRAM K., MAQBOOL Q., SELVAKESAVAN R.K., KRUSZKA D., KACHLICKI P., FRANKLIN G. Secondary metabolites in the green synthesis of metallic nanoparticles. Materials, **11** (6), 1, **2018**.
6. AGARWAL H., KUMAR S.V., RAJESH KUMAR S. A review on green synthesis of zinc oxide nanoparticles–An eco-friendly approach. Resource-Efficient Technologies, **3** (4), 406, **2017**.
7. THIND S., HUSSAIN I., RASHEED R., ASHRAF M.A., PERVEEN A., DITTA A., HUSSAIN S., KHALIL N.,

ULLAH Z., MAHMOOD Q. Alleviation of Cd stress by silicon nanoparticles during different phenological stages of Ujala wheat variety. Arabian Journal of Geosciences, **14**, 1028, **2021**.

8. REHANA D., MAHENDIRAN D., SENTHIL KUMAR R., KALILURRAHIMAN A. Evaluation of antioxidant and anticancer activity of copper oxide nanoparticles synthesized using medicinally important plant extracts. Biomedicine & Pharmacotherapy, **89**, 1067, **2017**.

9. RAHMAN S.S.U., QURESHI M.T., SULTANA K., REHMAN W., KHAN M.Y., ASIF M.H., SULTANA N. Single-step growth of iron oxide nanoparticles and their use as glucose biosensor. Results in Physics, **7**, 4451, **2017**.

10. JJAGWE J., OLUPOT P.W., MENYA E., KALIBBALA H.M. Synthesis and Application of Granular Activated Carbon from Biomass Waste Materials for Water Treatment: A Review. Journal of Bioresources and Bioproducts, **6** (4), 292, **2021**.

11. BERGNA D., HU T., PROKKOLA H., ROMAR H., LASSI U. Effect of Some Process Parameters on the Main Properties of Activated Carbon Produced from Peat in a Lab-Scale Process. Waste Biomass Valor, **11**, 2837, **2020**.

12. NJEWA J.B., VUNAIN E., BISWICK T. Synthesis and Characterization of Activated Carbons Prepared from Agro-Wastes by Chemical Activation. Journal of Chemistry, **13**, 9975444, **2022**.

13. SALEEM J., SHAHID U.B., HIJAB M., MACKEY H., MCKAY G. Production and applications of activated carbons as adsorbents from olive stones. Biomass Conversion and Biorefinery, **9**, 775, **2019**.

14. COUTO G.M., DESSIMONI A.L.D.A., BIANCHI M.L., PERÍGOLO D.M., TRUGILHO P.F. Use of sawdust Eucalyptus sp. in the preparation of activated carbons. Ciência e Agrotecnologia, **36**, 69, **2012**.

15. WILLIAMS P.T., REED A.R. Development of activated carbon pore structure via physical and chemical activation of biomass fiber waste. Biomass and bioenergy, **30** (2), 144, **2006**.

16. YOSHIZAWA N., MARUYAMA K., YAMADA Y., ZIELINSKA-BLAJET M. XRD evaluation of CO2 activation process of coal-and coconut shell-based carbons. Fuel, **79** (12), 1461, **2000**.

17. ALLWAR A., HARTATI R.I. Effect of nitric acid treatment on activated carbon derived from oil palm shell. AIP Conference Proceedings, **1823**, 020129, **2017**.

18. CUHADAROGLU D., UYGUN O.A. Production and characterization of activated carbon from bituminous coal by chemical activation. African Journal of Biotechnology, **7** (20), **2008**.

19. MORENO-CASTILLA C., FERRO-GARCIA M.A., JOLY J.P., BAUTISTA-TOLEDO I., CARRASCO-MARIN F., RIVERA-UTRILLA J. Activated carbon surface modifications by nitric acid, hydrogen peroxide, and ammonium peroxydisulfate treatments. Langmuir, **11** (11), 4386, **1995**.

20. LILLO-RÓDENAS M.A., CAZORLA-AMORÓS D., LINARES-SOLANO A. Understanding chemical reactions between carbons and NaOH and KOH: an insight into the chemical activation mechanism. Carbon, **41** (2), 267, **2003**.

21. GUO Y., ROCKSTRAW D.A. Physical and chemical properties of carbons synthesized from xylan, cellulose, and Kraft lignin by H3PO4 activation. Carbon, **44** (8), 1464, **2006**.

22. YAGMUR E., GOKCE Y., TEKIN S., SEMERCI N. I., AKTAS Z. Characteristics and comparison of activated carbons prepared from oleaster (Elaeagnus angustifolia L.) fruit using KOH and ZnCl2. Fuel, **267**, 117232, **2020**.

23. SAKA C. BET TG–DTG, FT-IR, SEM, iodine number analysis, and preparation of activated carbon from acorn shell by chemical activation with ZnCl₂. Journal of Analytical and Applied Pyrolysis, **95**, 21, **2012**.

24. VUNAIN E., KENNETH D., BISWICK T. Synthesis and characterization of low-cost activated carbon prepared from Malawian baobab fruit shells by H3PO4 activation for removal of Cu(II) ions: equilibrium and kinetics studies. Applied Water Science, **7**, 4301, **2017**.

25. MEHMOOD S., RIZWAN M., BASHIR S., DITTA A., AZIZ O., YONG L.Z., DAI Z., AKMAL M., AHMED W., ADEEL M., IMTIAZ M., TU S. Comparative Effects of Biochar, Slag and Ferrous–Mn Ore on Lead and Cadmium Immobilization in Soil. Bulletin of Environmental Contamination and Toxicology, **100** (2), 286, **2018**.

26. NASIR M., MUCHLISIN Z.A., SAIFUL S., SUHENDRAYATNA S., MUNIRA M., IQHRAMMULLAH M. Heavy Metals in the Water, Sediment, and Fish Harvested from the Krueng Sabee River Aceh Province, Indonesia. Journal of Ecological Engineering, **22** (9), 224, **2021**.

27. DITTA A. Role of Nanoclay Polymers in Agriculture: Applications and perspectives. *In* SURENDER K.S. (Ed.). Nanohybrids in environmental and biomedical applications. Taylor and Francis (CRC Press): USA. pp. 323, **2019**.

28. KANWAL U., IBRAHIM M., ABBAS F., YAMIN M., JABEEN F., SHAHZADI A., FAROOQUE A.A., IMTIAZ M., DITTA A., ALI S. Phytoextraction of Lead using a Hedge Plant [*Alternanthera bettzickiana* (Regel) G. Nicholson]: Physiological and Bio-chemical Alterations through Bioresource Management. Sustainability, **13** (9), 5074, **2021**.

29. DUMKOVÁ J., SMUTNÁ T., VRLÍKOVÁ L., LE COUSTUMER P., VEČEŘA Z., DOČEKAL B., MIKUŠKA P., ČAPKA L., FICTUM P., HAMPL A., BUCHTOVÁ M. Sub-chronic inhalation of lead oxide nanoparticles revealed their broad distribution and tissue-specific subcellular localization in target organs. Particle and Fibre Toxicology, **14** (1), 1, **2017**.

30. MEHMOOD S., SAEED D.A., RIZWAN M., KHAN M.N., AZIZ O., BASHIR S., IBRAHIM M., DITTA A., AKMAL M., MUMTAZ M.A., AHMED W., IRSHAD S., IMTIAZ M., TU S., SHAHEEN A. Impact of different amendments on biochemical responses of sesame (*Sesamum Indicum* L.) plants grown in lead-cadmium contaminated soil. Plant Physiology and Biochemistry, **132**, 345, **2018**.

31. AWUAL M.R. Mesoporous composite material for efficient lead(II) detection and removal from aqueous media. Journal of Environmental Chemical Engineering, **7** (3), 103124, **2019**.

32. SALMAN M.S., ZNAD H., HASAN M.N., HASAN M.M. Optimization of an innovative composite sensor for Pb(II) detection and capturing from water samples. Microchemical Journal, **160** (Part B), 105765, **2021**.

33. AWUAL M.R., ISLAM A., HASAN M.M., RAHMAN M.M., ASIRI A.M., KHALEQUE, M.A., SHEIKH, M.C. Introducing an alternate conjugated material for enhanced lead(II) capturing from wastewater. Journal of Cleaner Production, **224**, 920, **2019**.

34. DITTA A., ULLAH N. An update on nanotechnology and sustainable agriculture. In: Waqar Ahmed and Ehsan Nourafkan. Science and Applications of Nanoparticles. Jenny Stanford Publishing Pte. Ltd.: Singapore, pp. 159, **2022**.

35. KAKAVANDI B., JONIDI A., REZAEI R., NASSERI S., AMERI A., ESRAFILY A. Synthesis and properties of Fe3O4-activated carbon magnetic nanoparticles for removal of aniline from aqueous solution: equilibrium, kinetic and thermodynamic studies. Iranian Journal of Environmental Health Science & Engineering, **10**, 1, **2013**.

36. YAO S., SUN S., WANG S., SHI Z. Adsorptive removal of lead ion from aqueous solution by activated carbon/iron oxide magnetic composite. Indian Journal of Chemical Technology, **23**, 146, **2016**.

37. DANG V.B.H., DOAN H.D., DANG-VU T., LOHI A. Equilibrium and kinetics of biosorption of cadmium(II) and copper(II) ions by wheat straw. Bioresource Technology, **100** (1), 211, **2009**.

38. LEVANKUMAR L., MUTHUKUMARAN V., GOBINATH M.B. Batch adsorption and kinetics of chromium (VI) removal from aqueous solutions by *Ocimum americanum* L. seed pods. Journal of Hazardous Materials, **161**, 709, **2009**.

39. GANG M., VYAS S. Utilization of Ice Apple Shell Waste Nanocomposites for Removal of Chromium Ion from Aqueous Media. International Journal of Scientific Research and Engineering Development, **5** (5), 542, **2022**.

40. KRISHNAN K.A., ANIRUDHAN T.S. Removal of Cadmium (II) from Aqueous Solutions by Steam-Activated Sulphurised Carbon Prepared from Sugar Cane Bagasse Pith: Kinetics and Equilibrium Studies. Water SA, **29**, 147, **2003**.

41. YIN J., DENG C., YU Z., WANG X., XU G. Effective Removal of Lead Ions from Aqueous Solution Using Nano Illite/Smectite Clay: Isotherm, Kinetic, and Thermodynamic Modeling of Adsorption. Water, **10**, 210, **2018**.

42. KATARIA N, GARG V.K. Green synthesis of Fe3O4 nanoparticles loaded sawdust carbon for cadmium (II) removal from water: Regeneration and mechanism. Chemosphere, **208**, 818, **2018**.

43. SONI P., VYAS S. Removal of Iron from Aqueous Media using Surface Modified Soya Hulls: Optimizing Batch Adsorption Conditions. IJONS, **70**, 37817, **2022**.

44. KERA N.H, BHAUMIK M, PILLAY K, RAY S.S, MAITY A. Selective removal of toxic Cr(VI) from aqueous solution by adsorption combined with reduction at a magnetic nanocomposite surface. Journal of Colloid Interface Science, **503**, 214, **2017**.

45. MURTAZA G., DITTA A., AHMED Z., USMAN M., FAHEEM M., TARIQ A. Co-biosorption potential of *Acacia nilotica* bark in removing Ni and amino azo benzene from contaminated wastewater. Desalination and Water Treatment, **233**, 261, **2021**.

46. NETHAJI S., SIVASAMY A., MANDAL A.B. Preparation and characterization of corn cob activated carbon coated with nano-sized magnetite particles for the removal of Cr(VI). Bioresource Technology, **134**, 94, **2013**.